

Gravitino Decays and the Cosmological Lithium Problem in Light of the LHC Higgs and Supersymmetry Searches

Richard H. Cyburt¹, John Ellis^{2,3}, Brian D. Fields⁴,
Feng Luo², Keith A. Olive⁵ and Vassilis C. Spanos⁶

¹*Joint Institute for Nuclear Astrophysics (JINA), National Superconducting Cyclotron Laboratory (NSCL), Michigan State University, East Lansing, MI 48824, USA*

²*Theoretical Physics and Cosmology Group, Department of Physics, King's College London, London WC2R 2LS, UK*

³*TH Division, Physics Department, CERN, CH-1211 Geneva 23, Switzerland*

⁴*Departments of Astronomy and of Physics, University of Illinois, Urbana, IL 61801, USA*

⁵*William I. Fine Theoretical Physics Institute, School of Physics and Astronomy, University of Minnesota, Minneapolis, MN 55455, USA*

⁶*Institute of Nuclear and Particle Physics, NCSR "Demokritos", GR-15310 Athens, Greece*

Abstract

We studied previously the impact on light-element abundances of gravitinos decaying during or after Big-Bang nucleosynthesis (BBN). We found regions of the gravitino mass $m_{3/2}$ and abundance $\zeta_{3/2}$ plane where its decays could reconcile the calculated abundance of ${}^7\text{Li}$ with observation without perturbing the other light-element abundances unacceptably. Here we revisit this issue in light of LHC measurements of the Higgs mass and constraints on supersymmetric model parameters, as well as updates in the astrophysical measurements of light-element abundances. In addition to the constrained minimal supersymmetric extension of the Standard Model with universal soft supersymmetry-breaking masses at the GUT scale (the CMSSM) studied previously, we also study models with universality imposed below the GUT scale and models with non-universal Higgs masses (NUHM1). We calculate the total likelihood function for the light-element abundances, taking into account the observational uncertainties. We find that gravitino decays provide a robust solution to the cosmological ${}^7\text{Li}$ problem along strips in the $(m_{3/2}, \zeta_{3/2})$ plane along which the abundances of deuterium, ${}^4\text{He}$ and ${}^7\text{Li}$ may be fit with $\chi^2_{\min} \lesssim 3$, compared with $\chi^2 \sim 34$ if the effects of gravitino decays are unimportant. The minimum of the likelihood function is reduced to $\chi^2 < 2$ when the uncertainty on D/H is relaxed and < 1 when the lithium abundance is taken from globular cluster data.

March 2013

1 Introduction

The good agreement of the observed astrophysical abundances of the light elements with those calculated in standard Big-Bang nucleosynthesis (SBBN) [1] - [4] imposes interesting constraints on late-decaying massive particles, which are generic features of plausible extensions of the Standard Model, such as supersymmetry. There is even the possibility that the decays of massive particles could improve the agreement between calculation and observation, particularly in the case of ${}^7\text{Li}$ [5] - [15], whose abundance is calculated in standard BBN to be considerably higher than that observed in field halo stars or even globular clusters [4]. In a previous paper [11], we studied this possibility in the context of simple supersymmetric models with late-decaying massive gravitinos, taking into account the uncertainties in the astrophysical observations¹. We found that, for suitable values of the gravitino mass $m_{3/2}$ and abundance $\zeta_{3/2} \equiv m_{3/2}n_{3/2}/n_\gamma$, gravitino decays could reduce the combined χ^2 likelihood function for the deuterium, ${}^4\text{He}$ and ${}^7\text{Li}$ abundances from the SBBN value of ~ 32 to ~ 5.5 , thus offering a possible solution to the cosmological ${}^7\text{Li}$ problem.

Our previous analysis was in the context of the minimal supersymmetric extension of the Standard Model with soft supersymmetry-breaking mass parameters constrained to be universal at the GUT scale (the CMSSM). Moreover, we chose specific values of the CMSSM parameters that were allowed, even favoured, before the advent of the LHC searches for supersymmetry. These early parameter choices are now excluded by both the unsuccessful searches for supersymmetry at the LHC [16] and the determination of the Higgs mass at 125-126 GeV [17]. Partly for this reason, there is increased interest in alternatives to the CMSSM.

In this paper, we revisit our previous study including the WMAP9 estimate of the baryon density [18] and, where appropriate, updated estimates of the observational and nuclear-reaction uncertainties. In the absence of effects due to gravitino decays, we find that the SBBN value of the combined likelihood function $\chi^2 = 33.7$. Here we study the effects of gravitino decays in CMSSM models that are favoured in a recent global analysis of the CMSSM parameter space [19], and extend our study to include models with non-universal Higgs masses [20,21] (NUHM1) and models with universality imposed below the GUT scale [21,22] (subGUT).

In all cases, we find strips in the $(m_{3/2}, \zeta_{3/2})$ plane where the combined χ^2 likelihood function may be reduced to $\lesssim 3$ if the halo-star estimate of the ${}^7\text{Li}$ abundance is used, or < 1 if the globular-cluster estimate is used (to be compared with an SBBN value of ~ 23.8 if globular cluster ${}^7\text{Li}$ is used). If we relax the uncertainty in the D/H abundance (as may be warranted by the large dispersion in the data), we find that $\chi^2 \sim 1.2$. We conclude that the late decays of massive gravitinos offer a robust solution to the cosmological ${}^7\text{Li}$ problem. The likelihood function for the light-element abundances is minimized for a gravitino mass $m_{3/2}$ between ~ 4.6 and ~ 6.2 TeV and an abundance $\zeta_{3/2}$ in a narrow range between ~ 1.0 and $\sim 2.6 \times 10^{-10}$ GeV in the cases we study.

¹We also took into account the uncertainties in the relevant nuclear reaction rates, finding them to be subdominant, which is also the case here.

2 The Observed Light-Element Abundances and their Uncertainties

The ranges we adopt for the observed light-element abundances, follow largely those used in our previous work [23]. In that paper we delineated ranges that we considered acceptable, problematic, excluded and strongly excluded, as specified in Table 1, which is taken directly from [23]. In the subsequent figures, these ranges are left unshaded and coloured yellow, red and magenta, respectively. We now comment on the ranges of the light-element abundances that we consider to be preferred and use in the subsequent χ^2 analysis: more discussion can be found in [23].

Comparison with observation	D/H ($\times 10^{-5}$)	$^3\text{He}/\text{D}$	^4He	$^6\text{Li}/^7\text{Li}$	$^7\text{Li}/\text{H}$ $\times 10^{-10}$	$^9\text{Be}/\text{H}$ $\times 10^{-13}$
Strongly excluded	< 0.5	–	< 0.22	–	< 0.1	–
Excluded	< 1.0	–	< 0.23	–	< 0.2	–
Problematic	< 2.3	–	< 0.24	–	< 0.5	–
Acceptable	[2.3, 3.7]	[0.3, 1.0]	[0.24, 0.27]	< 0.05	[0.5, 2.75]	< 0.3
Problematic	> 3.7	> 1.0	> 0.27	> 0.05	> 2.75	> 0.3
Excluded	> 5.0	> 3.0	> 0.28	> 0.1	> 10	> 1.0
Strongly excluded	> 10	> 5.0	> 0.29	> 0.2	> 30	> 3.0

Table 1: *The ranges of light-element abundances whose comparisons with observation we consider, following [23], to be acceptable, problematic and (strongly) excluded, as shown in the unshaded/yellow/red/magenta regions in the Figures.*

D/H

We assume the central value [24]

$$\left(\frac{\text{D}}{\text{H}}\right)_p = (3.01 \pm 0.21) \times 10^{-5}, \quad (1)$$

corresponding to the deuterium abundance measured in 11 quasar absorption systems [25] and the error in the weighted mean. The SBBN value for D/H at the current baryon-to-photon ratio is $(2.51 \pm 0.17) \times 10^{-5}$. The combined uncertainty (theory and observation), is $\pm 0.27 \times 10^{-5}$. We also consider the sample variance in the data, which leads to a combined uncertainty of $\pm 0.70 \times 10^{-5}$ that is considerably less restrictive. Using the smaller error corresponds to being more conservative in claiming a solution to the ^7Li problem, whereas the more relaxed version of the D/H constraint corresponds to a more conservative approach to excluding scenarios. We note that we have taken a conservative approach in that we have not included the recent measurement of D/H in [26], as the spectrum suffers from the lack of a visible Lyman α emission feature since the absorber and emitter are at the same redshift.

Inclusion of this point would bring the mean downward (to 2.65×10^{-5}) with (in our view) an unrealistically small uncertainty of 0.11×10^{-5} (and sample variance of 0.36×10^{-5}). Furthermore, until several such measurements confirm the precision of this value, we cannot be assured that no *in situ* destruction of D/H has taken place, given the dispersion in the extant data [24].

${}^3\text{He}/\text{D}$

As discussed in [23], we expect the ratio ${}^3\text{He}/\text{D}$ [27] to be a monotonically increasing function of time, and therefore consider the solar ratio ${}^3\text{He}/\text{D} \simeq 1$ [28] to be a conservative upper bound on the BBN ratio. As we see later, this constraint is satisfied comfortably within all the region of interest, so we do not include it in our global χ^2 function, and hence do not need to assign an uncertainty.

${}^4\text{He}$

Following [23], we use the estimate [29]

$$Y_p = 0.2534 \pm 0.0083 \quad (2)$$

based on an analysis of the regression of Y vs. O/H . This should be compared to the SBBN value of 0.2487 ± 0.0002 .

${}^6\text{Li}/{}^7\text{Li}$

As in [23], we assign an upper limit ${}^6\text{Li}/{}^7\text{Li} < 0.05$, and (like the ${}^3\text{He}/\text{D}$ constraint) do not include it in our global χ^2 function.

${}^7\text{Li}/\text{H}$

The cosmological ${}^7\text{Li}$ problem [4] refers to the discrepancy between the SBBN prediction of ${}^7\text{Li}/\text{H} = (5.11^{+0.71}_{-0.62}) \times 10^{-10}$ and observations [30]. We adopt here the observational range [31]

$$\left(\frac{{}^7\text{Li}}{\text{H}}\right)_{\text{halo}\star} = (1.23^{+0.34}_{-0.16}) \times 10^{-10}, \quad (3)$$

leading to a combined uncertainty that we take as $\pm 0.71 \times 10^{-10}$. We note, however, that the ${}^7\text{Li}$ abundance in globular cluster stars is reported to be a factor ~ 2 higher [32, 33]. In our analysis below, we also derive results assuming [32] ${}^7\text{Li}/\text{H} = (2.34 \pm 0.05) \times 10^{-10}$ with a combined uncertainty of $\pm 0.62 \times 10^{-10}$.

${}^9\text{Be}/\text{H}$

We note finally that ${}^9\text{Be}$ is also observed in halo dwarf stars, with an abundance that varies strongly with metallicity, see, e.g., [34]. The observation with the lowest metallicity has an $[\text{O}/\text{H}]$ value of about -2.5 with a ${}^9\text{Be}/\text{H}$ abundance of 3×10^{-14} . We consider this to be a conservative upper limit on the ${}^9\text{Be}/\text{H}$ abundance, while noting that there is one observation [35] of ${}^9\text{Be}$ with an abundance about 3 times lower. As in the cases of ${}^3\text{He}/\text{D}$ and ${}^6\text{Li}/{}^7\text{Li}$, we do not include this observable in our global χ^2 function.

Finally, we note that our SBBN results are based on the WMAP9 determination of the baryon density [18] that corresponds to a baryon-to-photon ratio of $\eta = (6.20 \pm 0.14) \times 10^{-10}$. WMAP9 also provides a value of the cold dark matter density that can be used as an upper limit on the possible cosmological density of supersymmetric dark matter neutralino particles χ produced through thermal freeze out and by gravitino decays: $\Omega_\chi h^2 \leq 0.1138 \pm 0.0045$. In all of the models considered below, the relic density of neutralinos from thermal annihilations has been adjusted to yield the central WMAP value of $\Omega_\chi h^2 = 0.1138$ using the `SSARD` code [36], so all the neutralinos produced by gravitino decays contribute to the global χ^2 we define below.

3 Supersymmetric Models Studied

We have studied the light-element abundances in ten different supersymmetric models that respect the LHC and other current constraints.

Four of these models are taken from [19]², which studied the parameter spaces of the CMSSM and the NUHM1, taking into account not only the direct searches for supersymmetry via missing-transverse-energy events at the LHC [16], but also the mass measured for the Higgs boson discovered by ATLAS and CMS [17] and searches for the rare decay $B_s \rightarrow \mu^+ \mu^-$ [37]³ and the XENON100 direct search for dark matter scattering [40]. Ref. [19] found two well-defined and almost equally good local minima of the global likelihood function for the CMSSM, with quite distinct values of the scalar and gaugino soft supersymmetry-breaking parameters, m_0 and $m_{1/2}$, and the ratio of Higgs v.e.v.s, $\tan\beta$. Their values at the local best fits are shown in the first few columns of the first two rows in Table 2. The first of these points lies on a strip where the density of the lightest supersymmetric particle (LSP), the neutralino χ , is brought into the WMAP range by coannihilations with the nearly-degenerate next-to-lightest sparticle, the lighter stau $\tilde{\tau}_1$. The second point is located in a rapid-annihilation funnel where s-channel annihilations through heavy Higgses control the relic density. We also list the corresponding best-fit values for the trilinear soft supersymmetry-breaking parameter, A_0 , at the GUT scale, and note the positive sign assumed in [19] for the Higgs mixing parameter, μ , whose numerical value is fixed by the electroweak vacuum conditions in the CMSSM. The next two rows of Table 2 list the corresponding parameters for the best fit adapted from [19] in the NUHM1 framework, and a representative good fit with larger values of $m_0, m_{1/2}$ and $\tan\beta$. In these cases the corresponding values of μ are not fixed by the electroweak vacuum conditions, and we note their fit values.

²Their parameters are adapted for study using the `SSARD` code [36].

³The results in [19] are very little affected by incorporation of the recent measurement of $\text{BR}(B_s \rightarrow \mu^+ \mu^-)$ by the LHCb Collaboration [38], whose central value is quite close to the combination of previous data, and very consistent with the predictions of the CMSSM and NUHM1 fits in [19]: see <http://mastercode.web.cern.ch/mastercode/> for this and other current results from the Mastercode group. The best-fit models of [19] are also compatible with the preliminary constraints from LHC 8-TeV data [39].

ID	Model	Ref	$m_{1/2}$	m_0	A_0	$\tan \beta$	μ	m_χ	m_h	$m_{3/2}$	$\zeta_{3/2}$	$\tau_{3/2}$	χ^2_{\min}
1	CMSSM	[19]	905	361	1800	16	> 0	395	123.8	4560	1.5×10^{-10}	208	2.81
2	CMSSM	[19]	1895	1200	1200	50	> 0	857	123.3	5520	1.8×10^{-10}	231	2.86
3	NUHM1	[19]	970	345	2600	15	2600	427	123.8	4600	1.2×10^{-10}	220	2.82
4	NUHM1	[19]	2800	1040	2100	39	3800	1288	124.0	6200	2.6×10^{-10}	276	3.14
5	CMSSM	Fig. 2d of [21]	1115	1000	2500	40	> 0	496	124.8	4800	1.6×10^{-10}	213	2.87
6	NUHM1	Fig. 5b of [21]	1175	1500	3000	40	500	499	125.9	5000	2.6×10^{-10}	188	2.86
7	NUHM1	Fig. 6b of [21]	1300	1000	2500	30	-550	550	125.5	4700	1.0×10^{-10}	258	2.87
8	subGUT CMSSM	Fig. 9c of [21]	2040	2200	5500	10	> 0	1554	126.7	5400	1.6×10^{-10}	214	2.96
9	subGUT mSUGRA	Fig. 10d of [21]	2400	4000	Polonyi	36	> 0	1099	125.4	6000	1.6×10^{-10}	239	2.91
10	subGUT mSUGRA	Fig. 10d of [21]	1700	2000	Polonyi	33	> 0	1110	124.0	5100	1.6×10^{-10}	219	2.89
11	CMSSM ^(a)	[19]	905	361	1800	16	> 0	395	123.8	4440	1.5×10^{-10}	230	1.25
12	CMSSM ^(b)	[19]	905	361	1800	16	> 0	395	123.8	4520	1.0×10^{-10}	215	0.52
13	CMSSM ^(c)	[19]	905	361	1800	16	> 0	395	123.8	4360	7.1×10^{-11}	245	0.37

Table 2: *The models studied, with references, their input parameters and the corresponding values of m_h calculated using FeynHiggs [41] (which have an estimated theoretical uncertainty $\gtrsim 1.5$ GeV), the best-fit gravitino mass $m_{3/2}$ and abundance $\zeta_{3/2}$, and the minimum χ^2 in a global fit to the observed values of the light-element abundances. All mass parameters are expressed in GeV units, and the best-fit lifetime $\tau_{3/2}$ is in seconds. The subGUT model in Fig. 9c of [21] assumes $M_{in} = 10^9$ GeV, and those in Fig. 10d of [21] assume $M_{in} = 10^{10}$ GeV. In models 11 through 13, the χ^2 and best-fit values are computed using (a) the D/H sample variance uncertainty, (b) the ${}^7\text{Li}/\text{H}$ abundance as determined from globular clusters, and (c) both the D/H sample variance uncertainty and the globular cluster ${}^7\text{Li}/\text{H}$.*

We also show in Table 2 the corresponding masses of the lightest neutralino, χ , which is assumed in this paper to be the LSP and to constitute (the bulk of) the dark matter. We note that m_χ varies over a large range in the model fits. We also note the values calculated for the mass of the Higgs boson, m_h . Considering the theoretical uncertainties in the calculation of m_h [41], these values are consistent with the LHC measurement $m_h \sim 125$ to 126 GeV [17].

Although the first four rows in Table 2 include the best fits in the CMSSM and NUHM1, they do not exhaust the interesting possibilities offered by these models. Accordingly, we have also studied three other choices of CMSSM and NUHM1 parameters that are also compatible with the LHC constraints and offer complementary possibilities. The fifth row lists the parameters of a point towards the tip of the $\chi - \tilde{\tau}_1$ coannihilation strip for $\tan\beta = 40$ shown in Fig. 2d of [21], which has larger values of $m_0, m_{1/2}, A_0$ and m_χ than the best-fit point in the first row of Table 2. The sixth row illustrates a new possibility in the NUHM1 compared to the CMSSM shown in Fig. 5b of [21], namely the appearance at large $m_{1/2}$ of a band where the relic LSP density is brought down into the cosmological range because the make-up of the χ is in transition between a gaugino-like state at lower $m_{1/2}$ which has too high a relic density, and a Higgsino-like state at higher $m_{1/2}$, which has too low a relic density. The seventh row in Table 2 is an NUHM1 example with similar values of $m_0, m_{1/2}$ and $\tan\beta$, but with $\mu < 0$, which also lies along a transition strip, as seen in Fig. 6b of [21].

Finally, the next three rows in Table 2 illustrate possibilities if the soft supersymmetry-breaking parameters are universal at some scale $M_{in} < M_{GUT}$. The eighth row is a CMSSM example with $M_{in} = 10^9$ GeV, which is located along one of the rapid-annihilation funnels visible in Fig. 9c of [21]. The next two are mSUGRA-inspired examples with $M_{in} = 10^{10}$ GeV that are located on either side of the prominent rapid-annihilation funnel visible in Fig. 10d of [21]. In these cases supersymmetry is assumed to be broken by the simplest Polonyi superpotential, which specifies the corresponding value of A_0 . These examples populate regions of the $(m_{1/2}, m_0)$ plane that are not allowed in the CMSSM or the NUHM1 examples given above: they all have $m_{1/2} < m_0$ and large values of m_χ .

Since these examples exhibit several features not present in the specific CMSSM models studied previously, they serve to probe the robustness of the scenario for resolving the cosmological ${}^7\text{Li}$ problem proposed in [10, 11].

4 Results

In this Section we present in some detail results for the LHC-favoured CMSSM and NUHM1 models presented in the first four rows of Table 2, and then summarize results for the other six models.

In Fig. 1 we display the effects on the light-element abundances of the late decays of a gravitino with mass $m_{3/2} \in [2, 8]$ TeV and abundance $\zeta_{3/2} \in [10^{-14}, 10^{-7}]$ GeV. We show blocks of six panels for each of the models described in the first four rows of Table 2: lower-mass CMSSM (upper left), higher-mass CMSSM (upper right), lower-mass NUHM1 (lower left) and higher-mass NUHM1 (lower right). For each model, the upper left panel displays the effect of gravitino decays on the D/H ratio, the upper middle panel the effect on the ${}^3\text{He}/\text{D}$ ratio, the upper right panel the effect on the ${}^4\text{He}$ abundance, the lower left the effect

on the ${}^6\text{Li}/{}^7\text{Li}$ ratio, the lower middle the effect on the ${}^7\text{Li}/\text{H}$ ratio, and the lower right the effect on the ${}^9\text{Be}/\text{H}$ ratio. In each panel, the unshaded, yellow, red and magenta regions correspond to the ranges specified in Table 1. Solid shadings are used for regions with excess abundances, and hashed shadings for regions with low abundances.

The corresponding panels for the different models exhibit several common features. We note first that the D/H constraint typically excludes a large triangular region at small $m_{3/2}$ and large $\zeta_{3/2}$, but has no impact in the triangular region at large $m_{3/2}$ and small $\zeta_{3/2}$. Next we note that the ${}^3\text{He}/\text{D}$ constraint has no impact in any of these models. The impact of the ${}^4\text{He}$ constraint is always limited to a small region at relatively small $m_{3/2}$ and large $\zeta_{3/2}$ that lies within the region already excluded by the D/H ratio. The ${}^6\text{Li}/{}^7\text{Li}$ ratio typically excludes a band at smaller $m_{3/2}$ that is cut off at very small $\zeta_{3/2}$. The ${}^7\text{Li}/\text{H}$ ratio excludes not only a region at small $m_{3/2}$ and large $\zeta_{3/2}$, but also a region at large $m_{3/2}$ and small $\zeta_{3/2}$. In between, there is a banana-shaped region extending from $m_{3/2} \sim 3$ TeV upwards, where the ${}^7\text{Li}$ abundance falls within acceptable limits. The yellow shading at lower right in each of these panels reflects the existence of the cosmological ${}^7\text{Li}$ problem in standard BBN, and the unshaded banana indicates that this may be solved by the late decays of massive gravitinos. Finally, we note that the ${}^9\text{Be}/\text{H}$ constraint has impact only at small $m_{3/2}$ and large $\zeta_{3/2}$, in a region already excluded by the D/H ratio.

It is clear from this survey that, in all these four models, the most important constraints are those from the D/H and ${}^7\text{Li}/\text{H}$ ratios, and the issue is whether, within the unshaded ${}^7\text{Li}$ banana, there are model parameters where these constraints can be reconciled adequately.

This issue is addressed in Fig. 2 for the CMSSM and NUHM1 models described in the first four rows of Table 2. As in Fig. 1, the upper left panel is for the lower-mass CMSSM model, the upper right panel for the higher-mass CMSSM model, the lower left panel for the lower-mass NUHM1 model, and the lower right panel for the higher-mass NUHM1 model. In each panel, we display the values of D/H and ${}^7\text{Li}/\text{H}$ for a grid of points in the $(m_{3/2}, \zeta_{3/2})$ plane. The pattern of points in Fig. 2 arises as follows. Each of the loops (best visible at moderate D/H and ${}^7\text{Li}/\text{H}$) drops nearly vertically, goes through a minimum, and then rises towards high ${}^7\text{Li}/\text{H}$ and low D/H. A single loop represents a single value of $\zeta_{3/2}$. As seen in Fig. 1, scanning from low to high $m_{3/2}$ at fixed $\zeta_{3/2}$ generally takes us from high D/H to low D/H, and from high ${}^7\text{Li}/\text{H}$ to low ${}^7\text{Li}/\text{H}$ to somewhat higher ${}^7\text{Li}/\text{H}$. This leads to the loop behavior. For example the top “row” of blue points seen in the two panels on the left, correspond to $m_{3/2} = 2$ TeV and $\zeta_{3/2}$ increases from left to right. We see that the points examined in this scan grazes the inner ellipse representing the combined one- σ excursion of the observed D/H and ${}^7\text{Li}/\text{H}$ ratios.

The predominant feature in Fig. 2 is the correlation between lower ${}^7\text{Li}/\text{H}$ and higher D/H that is a common feature of many potential solutions to the ${}^7\text{Li}$ problem [24]. This is in fact a welcome feature as some enhancement in D/H is warranted when comparing the mean value from observations and the SBBN result. The red crosses represent the best-fit points in each of the four models, and lie close to the one- σ ellipses in all cases. We learn from these plots that the D/H and ${}^7\text{Li}/\text{H}$ observations can indeed be reconciled, with the D/H and ${}^7\text{Li}/\text{H}$ ratios lying within their combined one- σ observational band, somewhat above the central values given in Section 2.

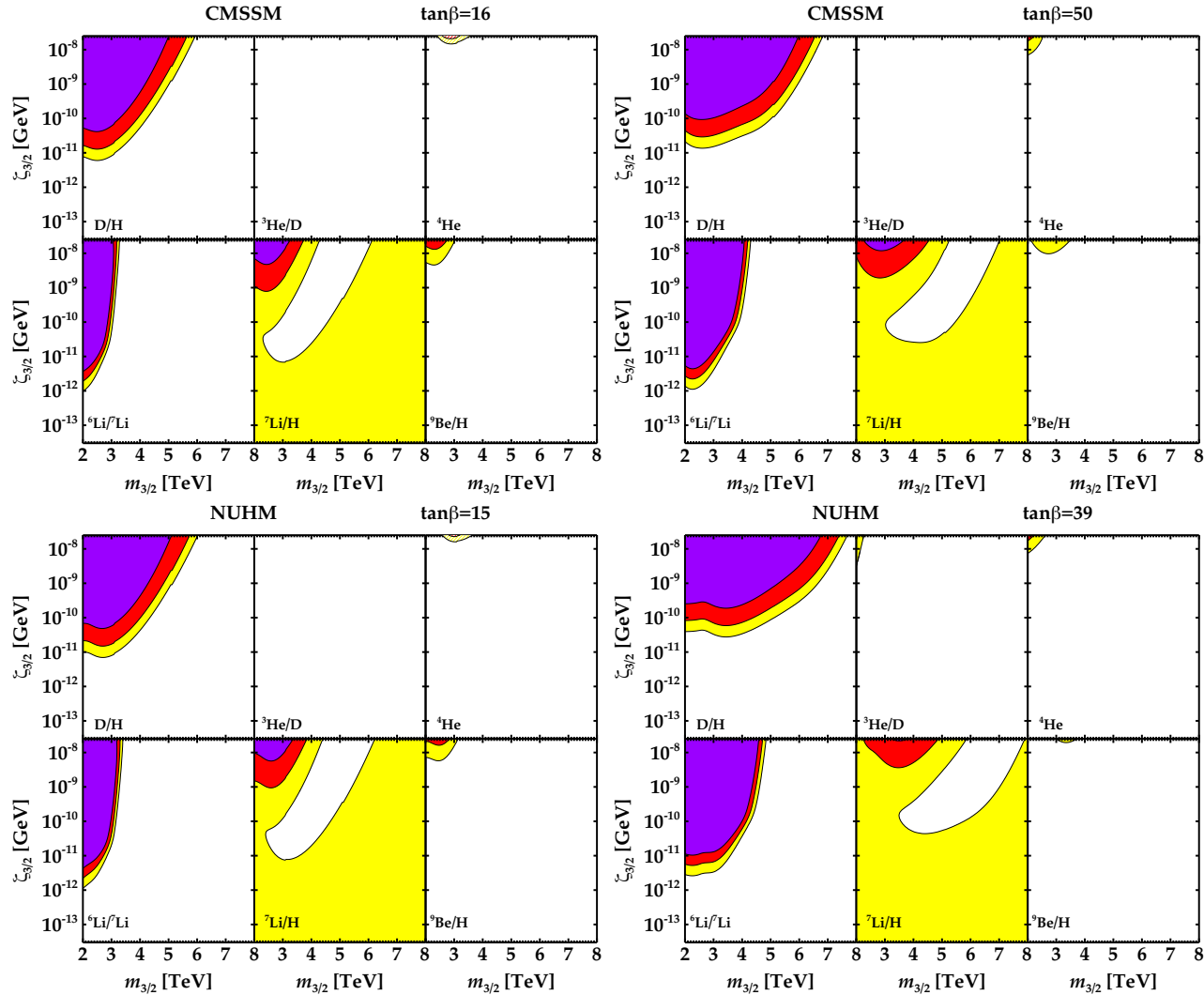


Figure 1: Plots of the effects on the light-element abundances of the decays of a gravitino with mass $m_{3/2} \in [2, 8]$ TeV and abundance $\zeta_{3/2} \in [10^{-14}, 10^{-7}]$ GeV. The results are displayed in blocks of six panels for each of the models described in the first four rows of Table 2. In each block, the upper left panel displays the effect on the D/H ratio, the upper middle panel that on the ${}^3\text{He}/\text{D}$ ratio, the upper right panel that on the ${}^4\text{He}$ abundance, the lower left that on the ${}^6\text{Li}/{}^7\text{Li}$ ratio, the lower middle that on the ${}^7\text{Li}/\text{H}$ ratio, and the lower right that on the ${}^9\text{Be}/\text{H}$ ratio. The unshaded regions in the panels are those allowed at face value by the ranges of the light-element abundances reviewed in Section 2, whilst the yellow, red and magenta regions correspond to progressively larger deviations from the central values of the abundances, as summarized in Table 1. Solid shadings are used for regions with excess abundances, and hashed shadings for regions with low abundances.

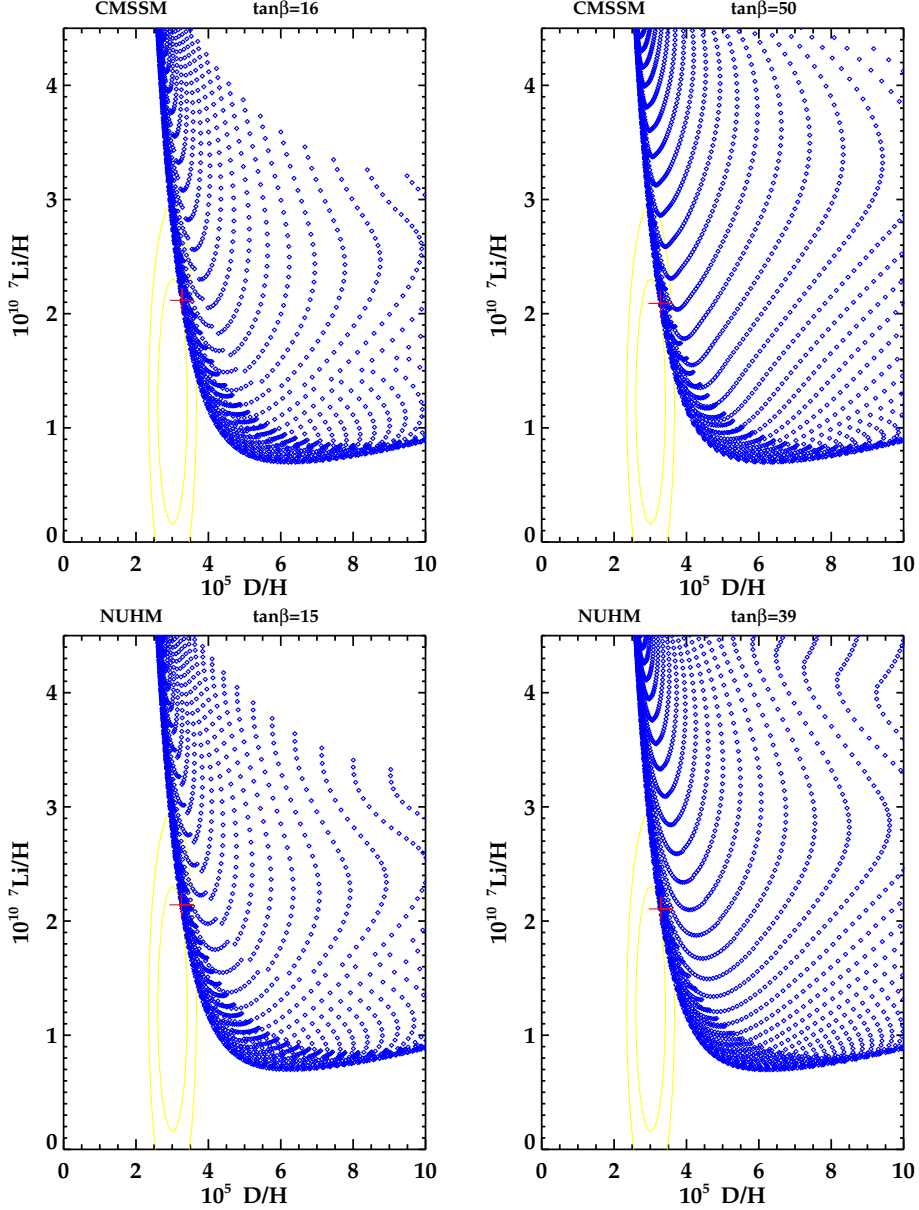


Figure 2: *Planes giving overviews of the D/H and ${}^7\text{Li}/H$ abundances obtainable in the models described in the first four rows of Table 2. The blue points show the values found in scans of the models for different values of $m_{3/2}$ and $\zeta_{3/2}$. The ellipses represent the one- and two- σ regions found by combining the D and ${}^7\text{Li}$ constraints reviewed in Section 2. The red cross marks the best fit found in each model.*

The broader issue of compatibility with all the constraints from light-element abundances is addressed in Fig. 3, which explores the mutual compatibility of all the light-element constraints in the $(m_{3/2}, \zeta_{3/2})$ planes for the models described in the first four rows of Table 2. In each case, the magenta region is where one or more calculated abundance lies within a

‘strongly-excluded’ range specified in Table 1, whereas in the red region the largest deviation is in an ‘excluded’ range, and in the yellow region the largest deviation is in a ‘problematic’ range. In each panel, we see that there is a strongly excluded magenta region at smaller $m_{3/2}$ and larger $\zeta_{3/2}$ (where there are deviations for D/H and some other abundances) and a disfavoured region at larger $m_{3/2}$ and smaller $\zeta_{3/2}$ (where the ${}^7\text{Li}$ abundance is similar to that in standard BBN) separated by an unshaded banana-shaped strip where no calculated light-element abundance disagrees significantly with observation. While the exact location and shape of the unshaded banana differs in each model, its presence is a generic feature we see not only in the four models displayed but in all ten we have studied.

As a refinement of this analysis of the compatibility between the different light-element constraints, we display in Fig. 4 contours of the global χ^2 function in the $(m_{3/2}, \zeta_{3/2})$ planes for the models listed in the first four rows of Table 2. The value of χ^2 is determined from

$$\chi^2 \equiv \left(\frac{Y_p - 0.2534}{0.0083} \right)^2 + \left(\frac{\text{D/H} - 3.01 \times 10^{-5}}{0.27 \times 10^{-5}} \right)^2 + \left(\frac{{}^7\text{Li/H} - 1.23 \times 10^{-10}}{0.71 \times 10^{-10}} \right)^2 + \left(\frac{\Omega_\chi^{(3/2)} h^2}{0.0045} \right)^2, \quad (4)$$

where

$$\Omega_\chi^{(3/2)} = \frac{m_\chi n_\gamma}{m_{3/2} \rho_c} \zeta_{3/2} \quad (5)$$

is the density of neutralinos produced in gravitino decays, ρ_c being the critical density of the Universe⁴. In each case, we see a narrow valley where $\chi^2 < 6.0$ (blue line), representing an acceptable solution to the cosmological ${}^7\text{Li}$ problem. In each case, the rise to $\chi^2 = 9.2$ (magenta line) is quite rapid, but the further rise at smaller $m_{3/2}$ and larger $\zeta_{3/2}$ (due to a combination of several constraints) is much more rapid than that at larger $m_{3/2}$ and smaller $\zeta_{3/2}$ (where it is due solely to the cosmological ${}^7\text{Li}$ problem). At high $\zeta_{3/2}$ the WMAP constraint plays a role in closing the contours for $\chi^2 = 6$ and 9.2 as well as the bend and flattening of the $\chi^2 = 33.7$ and 50 contours respectively. The black crosses in Fig. 4 indicate the best-fit points in the different scenarios: their properties $(m_{3/2}, \zeta_{3/2}, \tau_{3/2}, \chi_{\min}^2)$ are given in the first four rows of Table 2. We see that the best-fit gravitino mass varies between 4.6 and 6.2 TeV, and its abundance in the narrow range between 1.0 and 2.6×10^{-10} GeV. The best-fit gravitino lifetimes fall in an even more narrow range, $\tau_{3/2} \sim 210 - 280$ sec. Thus the models all show a close similarity in the best-fit gravitino abundance and lifetime values. This behavior is typical of decaying particle models we and other have studied, and indicates that these parameters exert the most sensitive control on the abundances of the light elements.

All four of the models have a χ_{\min}^2 of about 3, which represents a significant reduction from the SBBN value of 33.7⁵. However, there is also a price to be paid, in that we have added

⁴We note that it would in principle be possible to adapt the parameters of the models listed in Table 2 so that the density of thermally-produced neutralinos is below the central WMAP value, in which case the constraint on $\Omega_\chi^{(3/2)}$ would be relaxed. However, since this constraint is not important in the neighbourhoods of the best-fit points, we have not explored this option.

⁵The differences between these values and those found in [11] are due to a combination of factors, including the updated D/H abundance as well as the revised value of $\Omega_b h^2$ as well as the new supersymmetric model parameters.

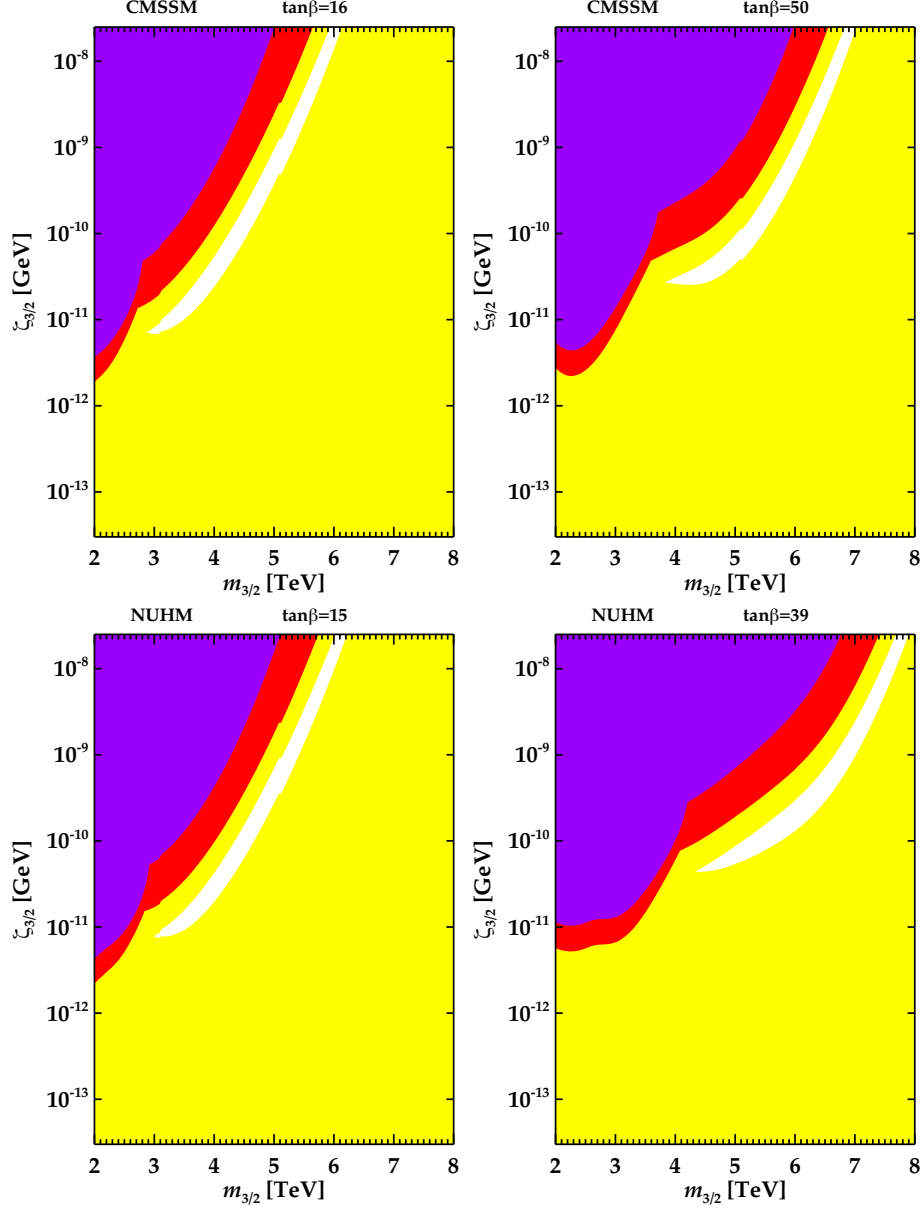


Figure 3: *Planes exploring the compatibility of all the light-element constraints in the $(m_{3/2}, \zeta_{3/2})$ planes for the models described in the first four rows of Table 2. In each case, the magenta region is where one or more calculated abundance lies within a ‘strongly-excluded’ range specified in Table 1, whereas in the red region the largest deviation is in an ‘excluded’ range, and in the yellow region the largest deviation is in a ‘problematic’ range. In the unshaded banana-shaped regions, there is no significant deviation in any of the calculated abundances.*

2 parameters ($m_{3/2}$ and $\zeta_{3/2}$) to achieve that benefit. As a result we have also decreased the number of degrees of freedom from 3 to 1. Nevertheless, the fit probability for χ^2 per degree of freedom of 3/1 is far superior to that for 33.7/3.

As also seen in Table 2, we have explored the effects of late-decaying massive gravitinos in six other scenarios: three other CMSSM and NUHM1 scenarios and three subGUT scenarios, all of them consistent with the current LHC and other constraints and representing different ways in which the relic χ density can be brought into the range favoured by WMAP and other experiments, as discussed earlier. The main features of our results for these scenarios are similar to those of the previous models shown and we list the parameters of the best fits in the 5th to the 10th row of Table 2. Each of them lies within the ranges found in the models discussed above.

We have studied effects in the first of the models in Table 2 under different assumptions on the D/H and ${}^7\text{Li}/\text{H}$ abundances, with the results shown in Fig. 5. In the left panel we show contours of the χ^2 function if the D/H constraint (1) is relaxed, keeping the same central value but assuming an uncertainty of $\pm 0.70 \times 10^{-5}$, given by the sample variance. In this case, the banana-shaped region with $\chi^2 < 6.0$ is significantly expanded, and the minimum value of $\chi^2 = 1.25$ (compared with the SBBN value of 30.7). The middle panel of Fig. 5 shows results obtained keeping the more restrictive uncertainty in D/H but assuming the globular cluster value for ${}^7\text{Li}/\text{H} = (2.34 \pm 0.62) \times 10^{-10}$. In this case, the ‘banana’ is even broader, and the minimum value of $\chi^2 = 0.52$ (compared with the SBBN value of 23.8). Finally, the right panel shows the effects of relaxing both the D/H and ${}^7\text{Li}/\text{H}$ constraints, and we see that the combined result is more similar to the result of relaxing the ${}^7\text{Li}/\text{H}$ constraint alone than that of relaxing the D/H constraint alone. In this case the minimum value of $\chi^2 = 0.37$ (compared with 20.8 in SBBN), demonstrating again that relaxing the ${}^7\text{Li}/\text{H}$ constraint is more important than relaxing the D/H constraint.

Table 3 presents light-element abundances predicted at the best-fit points for each of the models defined in Table 2. We see that all models select very similar best-fit values of D/H and ${}^7\text{Li}/\text{H}$, in line with the trends found in Fig. 2, namely a combination of the highest tolerable D/H and lowest tolerable ${}^7\text{Li}/\text{H}$. We also see that, in all models, there is no change in the helium abundance from its SBBN value. Finally, Table 3 shows the best-fit prediction for the relic χ abundance due to gravitino decays, $\Omega_\chi^{(3/2)} h^2$. These vary from $\sim (0.3 - 2) \times 10^{-3}$, and thus are at most about half of the observational uncertainty in $\Omega_{\text{cdm}} h^2$. The relic abundance constraint is therefore not a substantial contributor to the global χ^2 function in the regions of the best-fit points.

5 Summary and Conclusions

We had shown previously [11] that the late decays of massive gravitinos offered a possible solution of the cosmological ${}^7\text{Li}$ problem in a number of benchmark CMSSM scenarios proposed before the start-up of the LHC. The subsequent non-discovery of supersymmetry at the LHC [16], the discovery of a Higgs boson [17], the measurement of $B_s \rightarrow \mu^+ \mu^-$ [37] and the XENON100 dark-matter search experiment [40] have squeezed severely the allowed region of the CMSSM parameter space [19], and stimulating the exploration of alternative super-

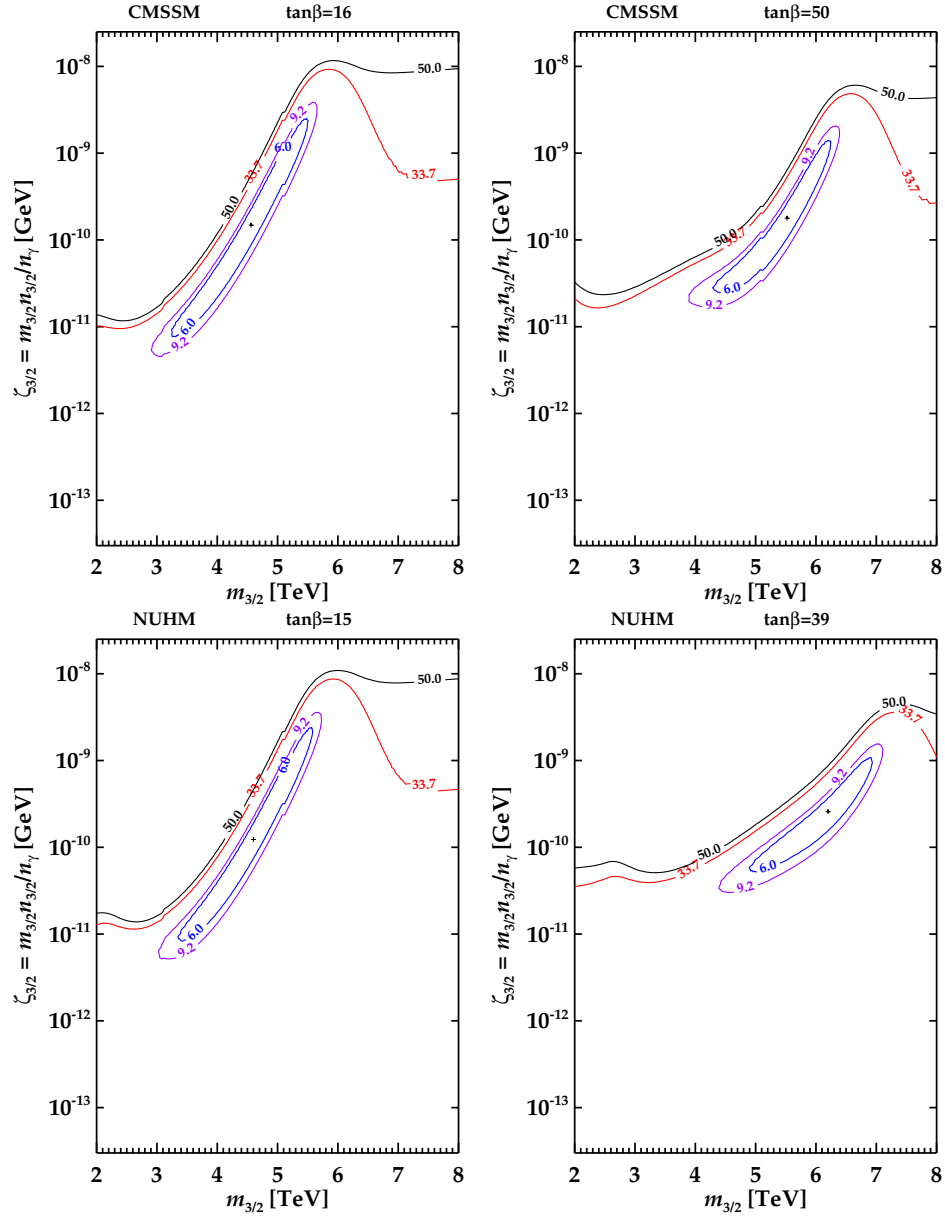


Figure 4: Contours of the χ^2 function in the $(m_{3/2}, \zeta_{3/2})$ planes for the models described in the first four rows of Table 2: $\chi^2 = 6.0$ (blue), 9.2 (magenta), 33.7 (red) and 50 (black). Also marked by black crosses are the best-fit points in the various models.

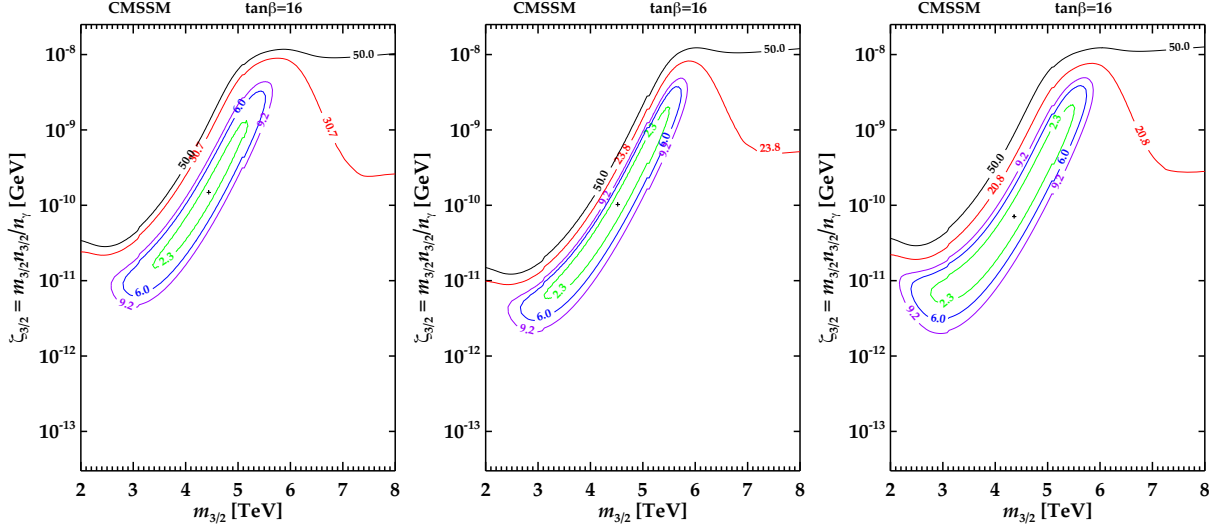


Figure 5: Contours of the χ^2 function in the $(m_{3/2}, \zeta_{3/2})$ planes for the low-mass CMSSM model described in the first row of Table 2 under different assumptions on the D/H and ${}^7\text{Li}/H$ abundances. In the left panel we relax the D/H constraint by using an increased uncertainty $\pm 0.70 \times 10^{-5}$, in the middle panel we use the globular cluster value for ${}^7\text{Li}/H = (2.34 \pm 0.05) \times 10^{-10}$, and in the right panel we combine these assumptions. The contours are coloured as follows: $\chi^2 = 2.3$ (green), $\chi^2 = 6.0$ (blue), $\chi^2 = 9.2$ (magenta), and $\chi^2 = 50$ (black). The red contour corresponds to the SBBN χ^2 for each case, namely 30.7, 23.8, and 20.8 for the left, middle, and right panels respectively. Also marked by black crosses are the best-fit points under these different assumptions.

symmetric scenarios such as NUHM1 models with non-universal Higgs masses and subGUT models in which soft supersymmetry-breaking masses are assumed to be universal at some scale below the GUT scale [21]. In this paper, we have explored the most favoured sets of CMSSM and NUHM1 parameters not yet excluded by the LHC [19], as well as a number of alternative models within the NUHM1 and subGUT frameworks, as summarized in Table 2.

In contrast to the constraints on supersymmetric model parameters, the constraints on primordial light-element abundances have remained essentially unchanged since [11], as summarized in Table 1. Thus the cosmological ${}^7\text{Li}$ problem remains.

In this paper we have repeated the global χ^2 likelihood analysis of [11], and studied the regions of the gravitino parameters $(m_{3/2}, \zeta_{3/2})$ that offer the best prospects of solving the cosmological ${}^7\text{Li}$ problem. In all the models studied, we find global $\chi^2_{\min} \lesssim 3$ in the $(m_{3/2}, \zeta_{3/2})$ plane and therefore the cosmological ${}^7\text{Li}$ problem can be regarded even more effectively solved than in [11]. Typical ranges of the gravitino parameters are $4.6 \text{ TeV} < m_{3/2} < 6.2 \text{ TeV}$ and $1.0 \times 10^{-10} \text{ GeV} < \zeta_{3/2} < 2.6 \times 10^{-10} \text{ GeV}$.

In view of this persistence of the massive gravitino solution despite the impact of LHC results on the supersymmetric parameter space, we conclude that the late decays of massive gravitinos provide a robust solution to the cosmological ${}^7\text{Li}$ problem.

ID	Y_p	10^5 D/H	10^{10} ${}^7\text{Li}/\text{H}$	$\Omega_\chi^{(3/2)} h^2$	χ_{\min}^2
1	0.2487	3.27	2.12	5.0×10^{-4}	2.81
2	0.2487	3.28	2.09	1.1×10^{-3}	2.86
3	0.2487	3.26	2.14	4.4×10^{-4}	2.82
4	0.2487	3.29	2.11	2.1×10^{-3}	3.14
5	0.2487	3.32	2.01	6.5×10^{-4}	2.87
6	0.2487	3.27	2.11	1.0×10^{-3}	2.86
7	0.2487	3.29	2.08	4.7×10^{-4}	2.87
8	0.2487	3.25	2.16	1.8×10^{-3}	2.96
9	0.2487	3.31	2.04	1.2×10^{-3}	2.91
10	0.2487	3.28	2.09	1.4×10^{-3}	2.89
11	0.2487	3.55	1.63	5.1×10^{-4}	1.25
12	0.2487	3.10	2.50	3.5×10^{-4}	0.52
13	0.2487	3.15	2.40	2.5×10^{-4}	0.37

Table 3: *Predictions at the best-fit points for the models defined in Table 2 for light-element abundances and the neutralino abundance $\Omega_\chi^{(3/2)} h^2$ arising from gravitino decays.*

Acknowledgments

The work of R.H.C. was supported by the U.S. National Science Foundation Grant PHY-08-22648 (JINA). The work of J.E. and F.L. was supported in part by the London Centre for Terauniverse Studies (LCTS), using funding from the European Research Council via the Advanced Investigator Grant 267352. The work of B.D.F. was partially supported by the U.S. National Science Foundation Grant PHY-1214082. The work of K.A.O. was supported in part by DOE grant DE-FG02-94ER-40823 at the University of Minnesota. The work of V.C.S. was supported by Marie Curie International Reintegration grant SUSYDM-PHEN, MIRG-CT-2007-203189.

References

- [1] R. H. Cyburt, B. D. Fields and K. A. Olive, *New Astron.* **6** (2001) 215 [arXiv:astro-ph/0102179]; R. H. Cyburt, B. D. Fields and K. A. Olive, *Phys. Lett. B* **567**, 227 (2003) [astro-ph/0302431].
- [2] A. Coc, E. Vangioni-Flam, P. Descouvemont, A. Adahchour and C. Angulo, *Astrophys. J.* **600** (2004) 544 [arXiv:astro-ph/0309480]; A. Cuoco, F. Iocco, G. Mangano, G. Miele, O. Pisanti and P. D. Serpico, *Int. J. Mod. Phys. A* **19** (2004) 4431 [arXiv:astro-ph/0307213]; B. D. Fields and S. Sarkar in: J. Beringer *et al.* [Particle Data Group Collaboration], *Phys. Rev. D* **86**, 010001 (2012); P. Descouvemont, A. Adahchour, C. Angulo, A. Coc and E. Vangioni-Flam, *ADNDT* **88** (2004) 203 [arXiv:astro-ph/0407101]; P. D. Serpico, S. Esposito, F. Iocco, G. Mangano, G. Miele and O. Pisanti, *JCAP* **0412**, 010 (2004) [arXiv:astro-ph/0408076]; A. Coc, S. Goriely, Y. Xu, M. Saimpert and E. Vangioni, *Astrophys. J.* **744**, 158 (2012) [arXiv:1107.1117 [astro-ph.CO]].
- [3] R. H. Cyburt, *Phys. Rev. D* **70**, 023505 (2004) [arXiv:astro-ph/0401091].
- [4] R. H. Cyburt, B. D. Fields and K. A. Olive, *JCAP* **0811**, 012 (2008) [arXiv:0808.2818 [astro-ph]].
- [5] M. H. Reno and D. Seckel, *Phys. Rev. D* **37** (1988) 3441.
- [6] K. Jedamzik, *Phys. Rev. D* **70** (2004) 063524 [arXiv:astro-ph/0402344]; K. Jedamzik, *Phys. Rev. D* **70** (2004) 083510 [arXiv:astro-ph/0405583].
- [7] M. Kawasaki, K. Kohri and T. Moroi, *Phys. Lett. B* **625** (2005) 7 [arXiv:astro-ph/0402490]; *Phys. Rev. D* **71** (2005) 083502 [arXiv:astro-ph/0408426].
- [8] K. Jedamzik, K. -Y. Choi, L. Roszkowski and R. Ruiz de Austri, *JCAP* **0607**, 007 (2006) [hep-ph/0512044]; D. Cumberbatch, K. Ichikawa, M. Kawasaki, K. Kohri, J. Silk and G. D. Starkman, *Phys. Rev. D* **76**, 123005 (2007) [arXiv:0708.0095 [astro-ph]].
- [9] K. Jedamzik and M. Pospelov, *New J. Phys.* **11**, 105028 (2009) [arXiv:0906.2087 [hep-ph]].
- [10] R. H. Cyburt, J. Ellis, B. D. Fields, F. Luo, K. A. Olive and V. C. Spanos, *JCAP* **0910** (2009) 021 [arXiv:0907.5003 [astro-ph.CO]].
- [11] R. H. Cyburt, J. Ellis, B. D. Fields, F. Luo, K. A. Olive and V. C. Spanos, *JCAP* **1010** (2010) 032 [arXiv:1007.4173 [astro-ph.CO]].
- [12] M. Pospelov and J. Pradler, *Phys. Rev. Lett.* **106**, 121305 (2011) [arXiv:1010.4079 [astro-ph.CO]].
- [13] M. Pospelov and J. Pradler, *Ann. Rev. Nucl. Part. Sci.* **60**, 539 (2010) [arXiv:1011.1054 [hep-ph]].

- [14] M. Kawasaki and M. Kusakabe, Phys. Rev. D **83**, 055011 (2011) [arXiv:1012.0435 [hep-ph]].
- [15] D. Albornoz Vasquez, A. Belikov, A. Coc, J. Silk and E. Vangioni, Phys. Rev. D **86**, 063501 (2012) [arXiv:1208.0443 [astro-ph.CO]].
- [16] G. Aad *et al.* [ATLAS Collaboration], arXiv:1208.0949 [hep-ex]; S. Chatrchyan *et al.* [CMS Collaboration], JHEP **1210**, 018 (2012) [arXiv:1207.1798 [hep-ex]]; Phys. Rev. Lett. **109**, 171803 (2012) [arXiv:1207.1898 [hep-ex]].
- [17] G. Aad *et al.* [ATLAS Collaboration], Phys. Lett. B **716**, 1 (2012) [arXiv:1207.7214 [hep-ex]]; S. Chatrchyan *et al.* [CMS Collaboration], Phys. Lett. B **716**, 30 (2012) [arXiv:1207.7235 [hep-ex]].
- [18] G. Hinshaw, D. Larson, E. Komatsu, D. N. Spergel, C. L. Bennett, J. Dunkley, M. R.olta and M. Halpern *et al.*, arXiv:1212.5226 [astro-ph.CO].
- [19] O. Buchmueller, R. Cavanaugh, M. Citron, A. De Roeck, M. J. Dolan, J. R. Ellis, H. Flacher and S. Heinemeyer *et al.*, Eur. Phys. J. C **72**, 2243 (2012) [arXiv:1207.7315 [hep-ph]].
- [20] H. Baer, A. Mustafayev, S. Profumo, A. Belyaev and X. Tata, Phys. Rev. D **71**, 095008 (2005) [arXiv:hep-ph/0412059]; H. Baer, A. Mustafayev, S. Profumo, A. Belyaev and X. Tata, JHEP **0507** (2005) 065, hep-ph/0504001; J. R. Ellis, K. A. Olive and P. Sandick, Phys. Rev. D **78**, 075012 (2008) [arXiv:0805.2343 [hep-ph]].
- [21] J. Ellis, F. Luo, K. A. Olive and P. Sandick, arXiv:1212.4476 [hep-ph].
- [22] J. R. Ellis, K. A. Olive and P. Sandick, Phys. Lett. B **642**, 389 (2006) [hep-ph/0607002]; J. R. Ellis, K. A. Olive and P. Sandick, JHEP **0706**, 079 (2007) [arXiv:0704.3446 [hep-ph]]; J. R. Ellis, K. A. Olive and P. Sandick, JHEP **0808**, 013 (2008) [arXiv:0801.1651 [hep-ph]].
- [23] R. H. Cyburt, J. Ellis, B. D. Fields, F. Luo, K. A. Olive and V. C. Spanos, JCAP **1212** (2012) 037 [arXiv:1209.1347 [astro-ph.CO]].
- [24] K. A. Olive, P. Petitjean, E. Vangioni and J. Silk, MNRAS **426**, 1427 (2012) [arXiv:1203.5701 [astro-ph.CO]].
- [25] S. Burles and D. Tytler, Astrophys. J. **499**, 699 (1998) [arXiv:astro-ph/9712108]; S. Burles and D. Tytler, Astrophys. J. **507**, 732 (1998) [arXiv:astro-ph/9712109]; J. M. O’Meara, D. Tytler, D. Kirkman, N. Suzuki, J. X. Prochaska, D. Lubin and A. M. Wolfe, Astrophys. J. **552**, 718 (2001) [arXiv:astro-ph/0011179]; M. Pettini and D. V. Bowen, Astrophys. J. **560**, 41 (2001) [arXiv:astro-ph/0104474]; S. A. Levshakov, M. Dessauges-Zavadsky, S. D’Odorico and P. Molaro, Astrophys. J. **565**, 696 (2002) [astro-ph/0105529]; D. Kirkman, D. Tytler, N. Suzuki, J. M. O’Meara and D. Lubin, Astrophys. J. Suppl. **149**, 1 (2003) [arXiv:astro-ph/0302006]; J. M. O’Meara, S. Burles,

- J. X. Prochaska, G. E. Prochter, R. A. Bernstein and K. M. Burgess, *Astrophys. J.* **649**, L61 (2006) [arXiv:astro-ph/0608302]; M. Pettini, B. J. Zych, M. T. Murphy, A. Lewis and C. C. Steidel, *MNRAS* **391**, 1499 (2008) [arXiv:0805.0594 [astro-ph]]; R. Srianand, N. Gupta, P. Petitjean, P. Noterdaeme and C. Ledoux, *MNRAS* **405**, 1888 (2010) [arXiv:1002.4620 [astro-ph.CO]]; M. Fumagalli, J. M. O’Meara and J. X. Prochaska, *Science* **334** 1245 (2011) [arXiv:1111.2334 [astro-ph.CO]]; P. Noterdaeme, S. Lopez, V. Dumont, C. Ledoux, P. Molaro and P. Petitjean, *Astron. Astrophys.* **542**, 33 (2012) [arXiv:1205.3777 [astro-ph.CO]].
- [26] M. Pettini and R. Cooke, *MNRAS* **425**, 2477 (2012) [arXiv:1205.3785 [astro-ph.CO]].
- [27] G. Sigl, K. Jedamzik, D. N. Schramm and V. S. Berezinsky, *Phys. Rev. D* **52** (1995) 6682 [arXiv:astro-ph/9503094].
- [28] J. Geiss, in *Origin and Evolution of the Elements*, eds. N. Prantzos, E. Vangioni-Flam, and M. Casse, (Cambridge University Press, Cambridge), 89 (1993).
- [29] E. Aver, K. A. Olive and E. D. Skillman, *JCAP* **1204**, 004 (2012) [arXiv:1112.3713 [astro-ph.CO]].
- [30] F. Spite, M. Spite, *Astronomy & Astrophysics*, **115** (1982) 357; S. G. Ryan, J. E. Norris and T. C. Beers, *Astrophys. J.* **523**, 654 (1999) [arXiv:astro-ph/9903059]; W. Aoki *et al.*, *Astrophys. J.* **698**, 1803 (2009) [arXiv:0904.1448 [astro-ph.SR]]; L. Sbordone *et al.*, *Astron. Astrophys.* **522**, 26 (2010) [arXiv:1003.4510 [astro-ph.GA]].
- [31] S. G. Ryan, T. C. Beers, K. A. Olive, B. D. Fields, and J. E. Norris, *Astrophys. J. Lett.* **530** (2000) L57 [arXiv:astro-ph/9905211].
- [32] J. I. G. Hernandez *et al.*, *Astron. Astrophys.* **505**, L13 (2009) [arXiv:0909.0983 [astro-ph.GA]].
- [33] L. Pasquini and P. Molaro, *Astron. Astrophys.* **307**, 761 (1996); F. Thevenin, C. Charbonnel, J. A. d. Pacheco, T. P. Idiart, G. Jasiewicz, P. de Laverny and B. Plez, *Astron. Astrophys.* **373**, 905 (2001) [arXiv:astro-ph/0105166]; P. Bonifacio *et al.*, *Astron. Astrophys.*, **390**, 91 (2002) [arXiv:astro-ph/0204332]; P. Bonifacio, *Astron. Astrophys.* **395**, 515 (2002) [arXiv:astro-ph/0209434]; K. Lind, F. Primas, C. Charbonnel, F. Grundahl and M. Asplund, *Astron. Astrophys.* **503**, 545 (2009) [arXiv:0906.2876 [astro-ph.SR]].
- [34] A. M. Boesgaard, J. A. Rich, E. M. Levesque and B. P. Bowler, *Astrophys. J.* **743**, 140 (2011) [arXiv:1110.2823 [astro-ph.SR]].
- [35] H. Ito, W. Aoki, S. Honda and T. C. Beers, *Astrophys. J.* **698**, L37 (2009) [arXiv:0905.0950 [astro-ph.SR]].
- [36] Information about this code is available from K. A. Olive: it contains important contributions from T. Falk, A. Ferstl, F. Luo, G. Ganis, A. Mustafayev, J. McDonald, K. A. Olive, P. Sandick, Y. Santoso, V. Spanos, and M. Srednicki.

- [37] G. Aad *et al.* [ATLAS Collaboration], Phys. Lett. B **713**, 387 (2012) [arXiv:1204.0735 [hep-ex]]; T. Aaltonen *et al.* [CDF Collaboration], Phys. Rev. Lett. **107**, 239903 (2011) [Phys. Rev. Lett. **107**, 191801 (2011)] [arXiv:1107.2304 [hep-ex]]; updated results presented at Aspen in Feb. 2012 by M. Rescigno, <https://indico.cern.ch/getFile.py/access?contribId=28&sessionId=7&resId=1&materialId=slides&confId=143360>; S. Chatrchyan *et al.* [CMS Collaboration], Phys. Rev. Lett. **107**, 191802 (2011) [arXiv:1107.5834 [hep-ex]]; R. Aaij *et al.* [LHCb Collaboration], Phys. Lett. B **699** (2011) 330 [arXiv:1103.2465 [hep-ex]]; arXiv:1203.4493 [hep-ex]; For an official combination of the ATLAS, CMS and LHCb results, see: ATLAS, CMS, and LHCb Collaborations, <http://cdsweb.cern.ch/record/1452186/files/LHCb-CONF-2012-017.pdf>.
- [38] R. Aaij *et al.* [LHCb Collaboration], Phys. Rev. Lett. **110**, 021801 (2013) [arXiv:1211.2674 [hep-ex]].
- [39] ATLAS Collaboration, <http://cdsweb.cern.ch/record/1472710>; CMS Collaboration, <http://cdsweb.cern.ch/record/1460095/files/SUS-12-016-pas.pdf>.
- [40] E. Aprile *et al.* [XENON100 Collaboration], Phys. Rev. Lett. **107** (2011) 131302 [arXiv:1104.2549 [astro-ph.CO]].
- [41] G. Degrossi, S. Heinemeyer, W. Hollik, P. Slavich and G. Weiglein, Eur. Phys. J. C **28** (2003) 133 [arXiv:hep-ph/0212020]; S. Heinemeyer, W. Hollik and G. Weiglein, Eur. Phys. J. C **9** (1999) 343 [arXiv:hep-ph/9812472]; S. Heinemeyer, W. Hollik and G. Weiglein, Comput. Phys. Commun. **124** (2000) 76 [arXiv:hep-ph/9812320]; M. Frank *et al.*, JHEP **0702** (2007) 047 [arXiv:hep-ph/0611326]; See <http://www.feynhiggs.de>.